10.1109/ULTSYM.2015.0246

# Evaluation of the Morphological Parameters of Cancer Cells Using High-frequency Ultrasound and Photoacoustics

Michael J. Moore, Eric M. Strohm, and Michael C. Kolios*
Department of Physics
Ryerson University
Toronto, Ontario, Canada
*Email: mkolios@ryerson.ca

***Abstract*—A method for acquiring commonly used histological parameters from cultured cancer cells is presented. Morphological features of the HT-29 colorectal cancer, and the MCF-7 breast cancer cell lines were obtained using a hybrid ultra-high frequency acoustic/photoacoustic microscope. The radii of the cell and nucleus were measured and used to calculate the cell nucleus-to-cytoplasm (N:C) ratio. To determine the radius of the cell, ultrasound waves backscattered from the cell were fit to analytical solutions describing acoustic scattering from a fluid sphere. Cells were stained with DRAQ5, a dye that binds to DNA, to facilitate generation of photoacoustic signals from the cell nuclei. Photoacoustic signals measured from the nuclei were fit to analytical solutions to determine the nuclear radius. For the HT-29 cells, the mean nuclear and cell radii were $5.3 \pm 1.1$ μm and $7.0 \pm 0.8$ μm, respectively. For the MCF-7 cell line, the mean nucleus and cell radii were found to be $6.0 \pm 0.7$ μm and $7.7 \pm 0.9$ μm, respectively. The mean calculated N:C ratio for the HT-29 cells was $2.3 \pm 1.9$, and the mean N:C ratio for the MCF-7 cells was $1.9 \pm 1.0$.**

## I. Introduction

Cancer metastasis is the cause of approximately 90% of all cancer related fatalities [1]. The metastatic spread of the disease is initiated when tumour cells shed by the primary tumour intravasate and disseminate throughout the body via the circulatory system [2]. Recent research suggests that quantification of the number of circulating tumour cells (CTC) in a patient's blood sample has potential applications in cancer screening, prognosis evaluation, and treatment monitoring [3]–[7]. For these reasons, minimally invasive 'liquid biopsies' of blood samples for CTC enumeration are quickly gaining popularity [8].

Most conventional CTC detection methods are dependent upon the expression of CTC specific antigens on the cell surface. If these antigens are not expressed, or if the antigen binding sites are damaged during intravasation, these methods are rendered ineffective [7]. Alternative methods, including RT-PCR and qPCR, require that the cells in the blood sample be lysed. In this case, no further analysis (to determine where the cells originated from) is possible [9]. Finally, label-free CTC detection methods that use size or density differences have a low sensitivity due to the presence of large leukocytes in the blood [7].

When operating transducers with central frequencies in the hundreds of MHz, the wavelength of the emitted acoustic pulse is on the order of the diameter of an individual cell. In this regime, ultrasound (US) pulses backscattered from cells are encoded with information pertaining to the cell's size and morphology [10]. The power spectra of the backscattered waves can be fit to theoretical models predicting the acoustic scattering from fluid spheres in order to determine the size of the entire cell. In photoacoustics (PA), the absorption of laser light by chromophores within a sample induces a thermoelastic expansion and the generation of a PA wave. This emitted PA wave contains information pertaining to the size and morphology of the optically absorbing structure [11]. The analysis of the power spectra of these waves has previously been used to detect changes in the of morphology of red blood cells, and to determine the size of optically absorbing melanoma cells [10], [12].

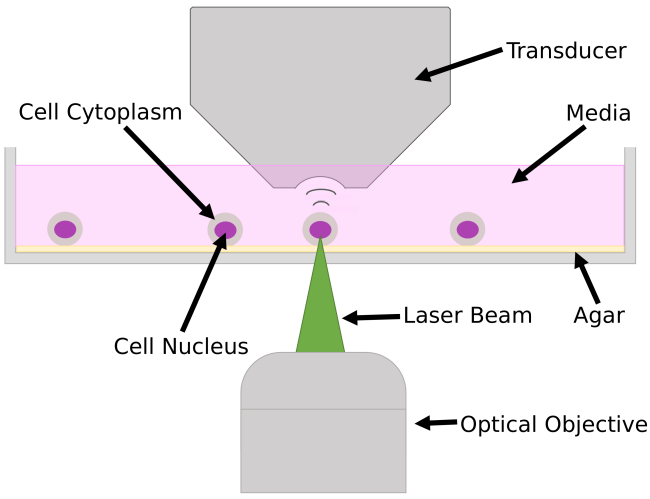


Fig. 1. Schematic of the experimental setup. In PA measurements, cells are irradiated with a pulsed laser focused on the sample by an optical objective. A transducer on the opposite side of the sample is used to record the emitted PA waves. For US measurements, no laser is used, and the transducer is operated in traditional pulse-echo mode.

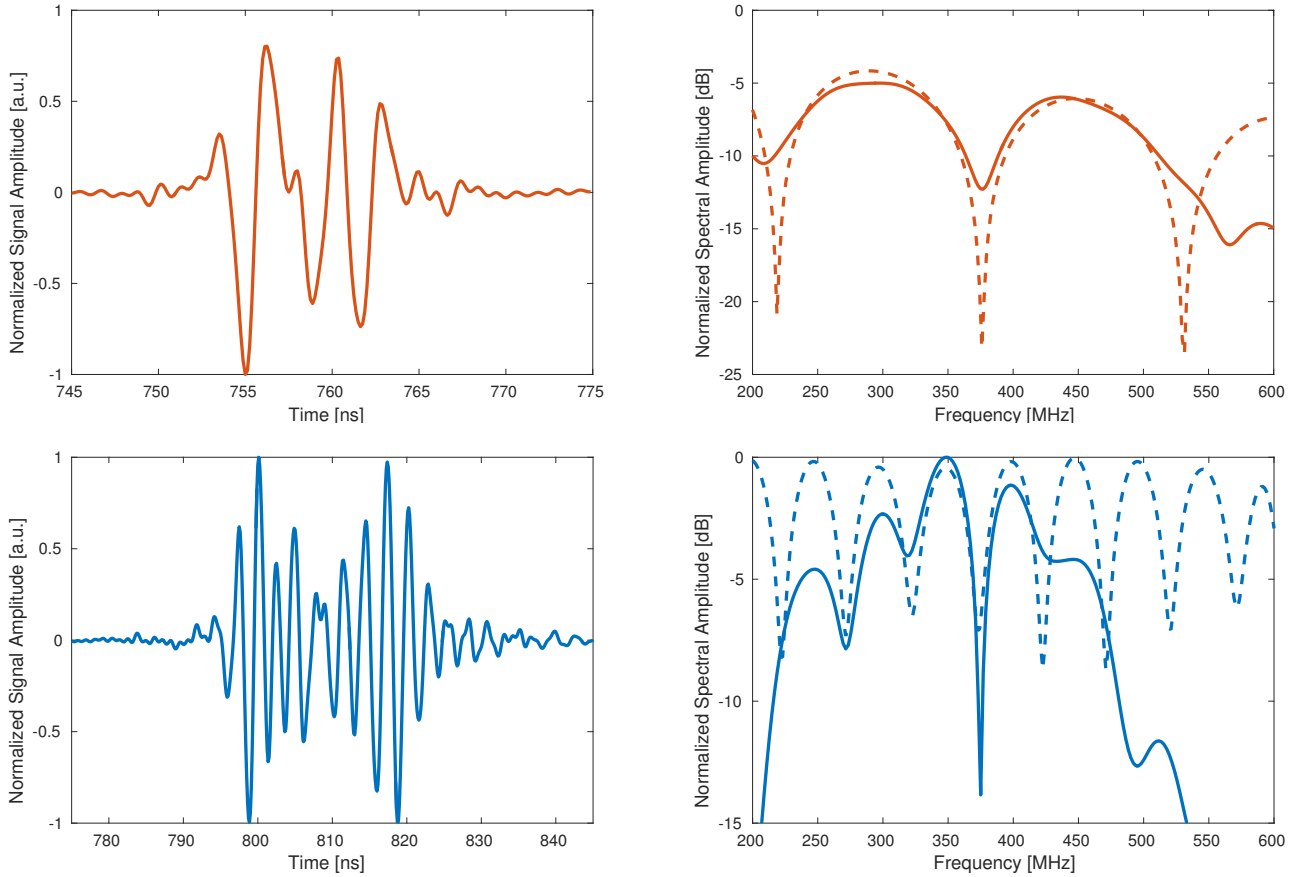


Fig. 2. Representative PA and US backscatter signals from a MCF-7 cell. Top: (Left) The measured PA signal emitted from the cell nucleus and (Right) the measured signal power spectrum (solid line) and theoretically predicted power spectrum (dashed line). Bottom: (Left) The measured US backscatter and (Right) the measured US signal power spectrum (solid line) and theoretically predicted power spectra (dashed line). The transducer bandwidth was from 300-450 MHz.

The nucleus-to-cytoplasmic (N:C) ratio, defined as the ratio of the cross sectional area of the nucleus to that of the surrounding cytoplasm, is commonly used to identify malignant cells in histopathology. A characteristic feature of malignant cells is a large nucleus surrounded by small amount of cytoplasm, resulting in a high N:C ratio [13]. In this study, we demonstrate that the morphological parameters and the N:C ratios of two different populations of cancerous cells (MCF-7 and HT-29) can be determined by a combined high-frequency US and PA approach. This method could potentially be used in liquid biopsies to discriminate between the smaller hematopoietic cells with low N:C ratios and the larger CTCs with high N:C ratios.

## II. Methods & Materials

### A. Cell Preparation

MCF-7 human breast cancer and HT-29 human colorectal cancer cells were cultured in Dulbeccos Modified Eagle Medium and McCoy's 5A Medium, respectively. Both media types were supplemented with 10% v/v fetal bovine serum. At confluence, cells were trypsinized and brought into suspension in their corresponding media. Optical absorption in cells is negligible in the visible spectrum, and so the DRAQ5 dye was used to facilitate PA signal generation from the cell nuclei. The cell suspension was incubated with DRAQ5 for 15 minutes at room temperature. The suspension was then centrifuged and the supernatant was aspirated. The pellet was resuspended in the appropriate cell culture media and HEPES buffer solution was added to reach a final concentration of 16% HEPES v/v. The suspension was transferred to a glass bottom petri dish (MatTek, USA) that had been coated with a thin layer of 1% agar. The agar was used to ensure that acoustic reflections from the glass would not interfere with emitted or backscattered acoustic waves.

### B. Cell Measurement

A reflection-mode scanning acoustic microscope (Kibero GmbH, Germany) modified to include a pulsed laser was used for cell interrogation. The microscope was outfitted with an US transducer with central frequency of 375 MHz and a -6 dB bandwidth of 150 MHz. For pulse-echo measurements, acoustic waves backscattered from individual cells were acquired at a pulse repetition rate of 121 kHz. Immediately

following pulse-echo measurements, PA measurements of the same cell were acquired. A pulsed 532 nm laser (TeemPhotonics, France) with a 330 ps pulse duration and a 4 kHz pulse repetition rate was directed through the microscope optical path, and a 10X optical objective (Olympus, Japan) was used to focus the laser beam onto the sample. The central axis of the transducer was aligned co-axially with the laser beam so that the focal spots of the transducer and laser beam overlapped. All acoustic and PA signals were sampled at 8 GS/s and averaged 200 times to increase SNR.

### C. Signal Processing & Feature Extraction

A bandpass filter from 100–800 MHz was used to eliminate noise from outside the transducer bandwidth. A Hamming window was used to select the US and PA signals, and a zero-padded Fourier transform was used to obtain the signal power spectrum. The radius of each cell was determined by fitting the measured US spectrum to the Frey and Goodman model for acoustic backscatter from a weakly scattering liquid sphere [14]. The radius of the nucleus was determined by fitting the measured PA signal spectrum to the analytical solution for the PA wave emitted by a spherical droplet [15]. In the fitting process, the speed of sound for all cells was assumed to be 1575 m/s [16]. For each cell, the N:C ratio was calculated via

$$\text{N:C} = \frac{N^2}{C^2 - N^2}, \tag{1}$$

where $N$ is the calculated nuclear radius, and $C$ is the calculated cell radius.

## III. Results

For this study, 25 HT-29 cells and 12 MCF-7 cells were measured. Representative measured signals and power spectra, as well as best fit theoretical curves are shown in Fig 2. For these proof-of-concept measurements, cells with a calculated nucleus radius greater than 95% of the calculated cell radius were excluded from the N:C calculations. In this regime, incremental increases in the nuclear radius cause large fluctuations in the calculated N:C ratio due to the subtraction operation in the denominator of Eq. 1. The fit nucleus and cell radii for the remaining cells are shown in Fig. 3. All calculated values are given in Table I.

### A. HT-29 Cells

The mean HT-29 cell radius calculated from the backscattered US signals was $7.0 \pm 0.8$ µm. The largest and smallest calculated cell radii were 9.2 µm and 5.9 µm, respectively. The mean nuclear radius calculated from the PA waves emitted from the cell nuclei was $5.3 \pm 1.1$ µm. The largest calculated nuclear radius was 7.4 µm and the smallest was 3.2 µm. The mean N:C ratio was $2.3 \pm 1.9$. The maximum and minimum calculated N:C ratios for the measured cells were 7.0 and 0.3, respectively.

### B. MCF-7 Cells

The mean MCF-7 cell radius calculated from the power spectra of the measured US signals was $7.7 \pm 0.9$ µm. The maximum and minimum calculated cell radii were 9.0 µm and 6.0 µm, respectively. The mean nuclear radius calculated from the acquired PA signals was $6.0 \pm 0.7$ µm. The maximum and minimum MCF-7 nucleus radii were 7.3 µm and 5.2 µm, respectively. The mean N:C ratio for the MCF-7 cells was $1.9 \pm 1.0$. The maximum and minimum N:C ratios were 3.6 and 0.7, respectively.

## IV. Discussion

There was good agreement between the US backscatter and PA spectra and theory over the bandwidth of the transducer, as shown in the representative fits in Fig. 2. On average, the HT-29 cells were slightly smaller than their MCF-7 counterparts; an observation which was also made by Frimat *et al* [17]. The mean calculated radius of the MCF-7 cells, $7.7 \pm 0.9$ µm, was in good agreement with the reported value of $8.1 \pm 1.5$ µm [18]. The mean nuclear radius of the MCF-7 cells, $6.0 \pm 0.7$ µm, was slightly larger than the value of $4.6 \pm 1.5$ µm found by Dahle *et al* [19]. The wider distribution in the fit radius of the HT-29 nuclei was reflected in a larger distribution of N:C ratios for the HT-29 cells compared to the MCF-7 cells. Despite this, both cell populations exhibited a large mean N:C ratio, which was expected due to their malignant nature. In the MCF-7 cells, the mean N:C ratio corresponded to a nucleus with radius equal to 81% of cell radius. In the HT-29 cells, the

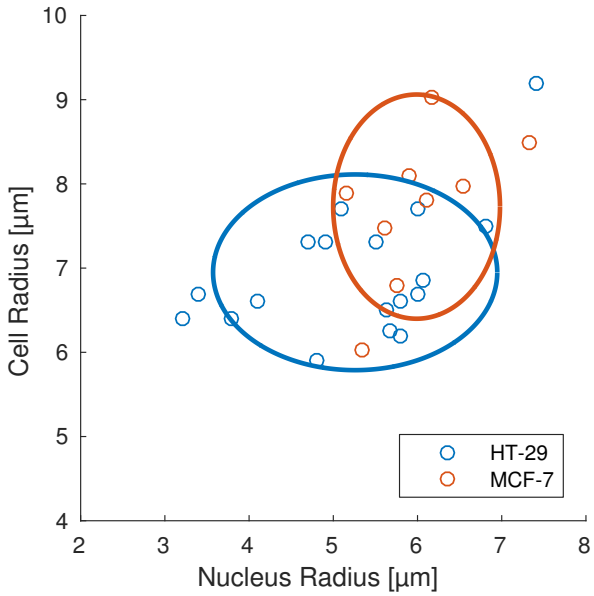


Fig. 3. The fit nucleus and cell radii for HT-29 cells (blue circles) and MCF-7 (orange circles). Each data point represents an individual cell. The blue and orange ellipses are centered about the mean nucleus and cell radius for the cell line of the corresponding colour. The horizontal and vertical axes of either ellipse are 1.5 times the standard deviation in the nucleus radius and cell radius, respectively.

TABLE I
PARAMETERS EXTRACTED FROM US/PA DATA

| Cell Line | HT-29 | | | MCF-7 | | |
|---|---|---|---|---|---|---|
| | Nuclear Radius (μm) | Cell Radius (μm) | N:C | Nuclear Radius (μm) | Cell Radius (μm) | N:C |
| Mean | $5.3 \pm 1.1$ | $7.0 \pm 0.8$ | $2.3 \pm 1.9$ | $6.0 \pm 0.7$ | $7.7 \pm 0.9$ | $1.9 \pm 0.1$ |
| Min | 3.2 | 5.9 | 0.3 | 5.2 | 6.0 | 0.7 |
| Max | 7.4 | 9.2 | 7.0 | 7.3 | 9.0 | 3.6 |

N:C equivalent nuclear radius was 84% of the cell radius. In comparison, the average nuclear radius of healthy mammalian cells is approximately 46% of the cell radius [20].

The scatter plot in Fig. 3 shows the fit nuclear and cell radii for each measured cell. Two ellipses centered at coordinates corresponding to the mean HT-29 and MCF-7 nucleus and cell radii were drawn with their horizontal axis and vertical axis equal to 1.5 times the standard deviation in nucleus and cell radius, respectively. For the number of cells analyzed in this study, significant overlap for these 'representative' regions was observed. If non-malignant cells were analyzed with this method, it is expected that little overlap would occur between malignant and non-malignant regions due to the large discrepancy in average cell N:C ratio.

## V. CONCLUSION

In this work, US signals backscattered from the cell, and PA signals emitted from the cell's nucleus were used to determine the radius of the cell and cell nucleus, respectively. Cells from two different cancerous cell lines were measured, and representative morphological regions for each cell type were established. The mean radius of the HT-29 colorectal cancer cells was $7.0 \pm 0.8$ μm, and the mean radius of the HT-29 nuclei was $5.3 \pm 1.1$ μm. The mean radius of the MCF-7 breast cancer cells was $7.7 \pm 0.9$ μm and the mean radius of the MCF-7 nuclei was $6.0 \pm 0.7$ μm. The mean calculated N:C ratios were $2.3 \pm 1.9$ and $1.9 \pm 1.0$ for HT-29 and MCF-7 cells, respectively. This method could be used to differentiate between malignant and non-malignant cells in a blood sample based on their calculated morphologic parameters.

## ACKNOWLEDGMENT

The authors would like to thank E. Berndl (Ryerson University) for her assistance with cell preparation. This research was supported in part be the Natural Sciences and Engineering Research Council of Canada, the Canadian Cancer Society, the Canadian Foundation for Innovation, and the Ontario Ministry for Research and Innovation.

## REFERENCES

[1] G. P. Gupta and J. Massagué, "Cancer Metastasis: Building a Framework," *Cell*, vol. 127, no. 4, pp. 679–695, 2006.

[2] K. Pantel and R. H. Brakenhoff, "Dissecting the metastatic cascade." *Nature reviews. Cancer*, vol. 4, no. 6, pp. 448–56, Jun. 2004.

[3] Y. Hüsemann, J. B. Geigl, F. Schubert, P. Musiani, M. Meyer, E. Burghart, G. Forni, R. Eils, T. Fehm, G. Riethmüller, and C. A. Klein, "Systemic spread is an early step in breast cancer." *Cancer cell*, vol. 13, no. 1, pp. 58–68, Jan. 2008.

[4] S. Nagrath, L. V. Sequist, S. Maheswaran, D. W. Bell, D. Irimia, L. Ulkus, M. R. Smith, E. L. Kwak, S. Digumarthy, A. Muzikansky, P. Ryan, U. J. Balis, R. G. Tompkins, D. A. Haber, and M. Toner, "Isolation of rare circulating tumour cells in cancer patients by microchip technology." *Nature*, vol. 450, no. 7173, pp. 1235–9, Dec. 2007.

[5] S. J. Cohen, C. J. Punt, N. Iannotti, B. H. Saidman, K. D. Sabbath, N. Y. Gabrail, J. Picus, M. Morse, E. Mitchell, M. C. Miller, G. V. Doyle, H. Tissing, L. W. M. M. Terstappen, and N. J. Meropol, "Relationship of circulating tumor cells to tumor response, progression-free survival, and overall survival in patients with metastatic colorectal cancer." *Journal of Clinical Oncology*, vol. 26, no. 19, pp. 3213–21, Jul. 2008.

[6] D. F. Hayes, M. Cristofanilli, G. T. Budd, M. J. Ellis, A. Stopeck, M. C. Miller, J. Matera, W. J. Allard, G. V. Doyle, and L. W. W. M. Terstappen, "Circulating tumor cells at each follow-up time point during therapy of metastatic breast cancer patients predict progression-free and overall survival." *Clinical Cancer Research*, vol. 12, no. 14 Pt 1, pp. 4218–24, Jul. 2006.

[7] M. Alunni-Fabbroni and M. T. Sandri, "Circulating tumour cells in clinical practice: Methods of detection and possible characterization," *Methods*, vol. 50, no. 4, pp. 289–297, 2010.

[8] C. Alix-Panabieres and K. Pantel, "Circulating tumor cells: Liquid biopsy of cancer," *Clinical Chemistry*, vol. 59, no. 1, pp. 110–118, Jan. 2013.

[9] P. Paterlini-Brechot and L. B. Naoual, "Circulating tumor cells (ctc) detection: Clinical impact and future directions," *Cancer Letters*, vol. 253, no. 2, pp. 180–204, 2007.

[10] E. M. Strohm and M. C. Kolios, "Circulating tumor cell detection using high frequency ultrasound and photoacoustics," *Cytometry Part A*, vol. 87, no. 8, pp. 741–749, 2015.

[11] G. J. Diebold, M. I. Khan, and S. M. Park, "Photoacoustic "signatures" of particulate matter: optical production of acoustic monopole radiation." *Science*, vol. 250, no. 4977, pp. 101–104, 1990.

[12] E. M. Strohm, E. S. L. Berndl, and M. C. Kolios, "Probing red blood cell morphology using high-frequency photoacoustics," *Biophysical Journal*, vol. 105, no. 1, pp. 59–67, 2013.

[13] L. Koss, *Koss' Diagnostic Cytology and Its Histopathologic Bases, 5ed.* Lippincott Williams & Wilkins, 2006.

[14] H. G. Frey and R. R. Goodman, "Acoustic Scattering from Fluid Spheres," *The Journal of the Acoustical Society of America*, vol. 40, no. 2, pp. 417–420, 1966.

[15] G. J. Diebold and P. J. Westervelt, "The photoacoustic effect generated by a spherical droplet in a fluid," *The Journal of the Acoustical Society of America*, vol. 84, no. 6, pp. 2245–2251, 1988.

[16] M. C. Kolios, E. M. Strohm, and G. J. Czarnota, "Acoustic Microscopy of Single Cells," in *Quantitative Ultrasound in Soft Tissues*, J. Mamou and M. Oelze, Eds. Springer, 2013, ch. 13, pp. 315–341.

[17] J.-P. Frimat, M. Becker, Y.-Y. Chiang, U. Marggraf, D. Janasek, J. G. Hengstler, J. Franzke, and J. West, "A microfluidic array with cellular valving for single cell co-culture," *Lab Chip*, vol. 11, no. 2, pp. 231–237, 2011.

[18] H. Reile, G. Bernhardt, M. Koch, H. Schonenberger, M. Hollstein, and F. Lux, "Chemosensitivity of human MCF-7 breast cancer cells to diastereoisomeric diaqua(1,2-diphenylethylenediamine) platinum(II) sulfates and specific platinum accumulation," *Cancer Chemotherapy and Pharmacology*, vol. 30, no. 2, pp. 113–122, 1992.

[19] J. Dahle, E. Kalanxhi, and N. Tisnek, "Dosimetry of a 238Pu-based $\alpha$-particle irradiator and its biological application in a study of the bystander effect," *Anticancer Research*, vol. 31, no. 6, pp. 2113–2120, 2011.

[20] B. Alberts, *Molecular Biology of the Cell, 5ed.* Garland Science, 2006.